Published in final edited form as:
Nat Cell Biol. 2017 May ; 19(5): 468–479. doi:10.1038/ncb3500.

CUL-2^{LRR-1} and UBXN-3/FAF1 drive replisome disassembly during DNA replication termination and mitosis

Remi Sonneville[1], **Sara Priego Moreno**[2], **Axel Knebel**[1], **Clare Johnson**[1], **C. James Hastie**[1], **Anton Gartner**[3], **Agnieszka Gambus**[2], and **Karim Labib**[1]

[1]MRC Protein Phosphorylation and Ubiquitylation Unit, School of Life Sciences, University of Dundee, Dow Street, Dundee, DD1 5EH, U.K.

[2]Institute of Cancer and Genomic Sciences, College of Medical and Dental Sciences, University of Birmingham, Edgbaston, Birmingham, B15 2TT, U.K.

[3]Centre for Gene Regulation and Expression, School of Life Sciences, University of Dundee, Dow Street, Dundee, DD1 5EH, U.K.

Abstract

Replisome disassembly is the final step of DNA replication in eukaryotes, involving the ubiquitylation and CDC48-dependent dissolution of the CMG helicase (Cdc45-MCM-GINS). Using *Caenorhabditis elegans* early embryos and *Xenopus* egg extracts, we show that the E3 ligase CUL-2^{LRR-1} associates with the replisome and drives ubiquitylation and disassembly of CMG, together with the CDC-48 co-factors UFD-1 and NPL-4. Removal of CMG from chromatin in frog egg extracts requires CUL2 neddylation, and our data identify chromatin recruitment of CUL2^{LRR1} as a key regulated step during DNA replication termination. Interestingly, however, CMG persists on chromatin until prophase in worms that lack CUL-2^{LRR-1}, but is then removed by a mitotic pathway that requires the CDC-48 co-factor UBXN-3, orthologous to the human tumour suppressor FAF1. Partial inactivation of *lrr-1* and *ubxn-3* leads to synthetic lethality, suggesting future approaches by which a deeper understanding of CMG disassembly in metazoa could be exploited therapeutically.

Chromosome replication in eukaryotes is initiated by the assembly of the CMG helicase at origins of DNA replication1, 2. CMG then controls the progression of DNA replication forks, by unwinding the parental DNA duplex to form the single-strand substrate for DNA

Correspondence should be addressed to a.gambus@bham.ac.uk or kpmlabib@dundee.ac.uk.

Data availability

Source data for Figure 6f, 7d and Supplementary figures 5b, 5c can be found in Supplementary Table 6. All other datasets generated during and/or analysed during the current study are available from the corresponding author on reasonable request.

Author Contributions

RS performed the experiments in Figures 1-5 and Figures S1-S4. SPM performed the experiments in Figures 6-7 and Figures S5. KL and Agnieszka Gambus conceived the project and designed experiments in collaboration with RS and SPM. AK and CJ produced recombinant CUL2-RBX1 and JH provided recombinant LRR1. Anton Gartner provided invaluable support in the early stages of the project. KL wrote the manuscript, with contributions and critical comments from the other authors.

Competing Financial Interests

The authors confirm that they have no competing financial interests.

Europe PMC Funders Author Manuscripts

polymerases3, 4. The CMG helicase forms the core of the eukaryotic replisome1, 5 and must remain associated with replication forks throughout elongation, since it cannot be reloaded6. The catalytic core of the helicase is formed by a hexameric ring of the MCM2-7 proteins, which is topologically trapped around the DNA template and is stabilised and activated by association with CDC45 and GINS1, 7.

The remarkably stable association of CMG with replication forks means that a specialized mechanism is needed to remove the helicase and trigger replisome disassembly during DNA replication termination8. In budding yeast and *Xenopus* egg extracts, the CMG helicase was found to be ubiquitylated on its Mcm7 subunit in a late step of DNA replication9–11, leading rapidly to a disassembly reaction that requires the CDC48/p97 AAA+ ATPase10, 11.

In *Saccharomyces cerevisiae*, the cullin 1-based E3 ligase SCF^{Dia2} associates with the replisome and is essential for CMG ubiquitylation and disassembly10, 12, 13. Orthologues of the F-box protein Dia2 are not apparent in metazoa, but a putative role for a metazoan cullin ligase during DNA replication termination was suggested by the fact that CMG ubiquitylation and disassembly are inhibited in *Xenopus* egg extracts11 by the neddlylation inhibitor MLN492414, since the major role of neddylation is to activate cullin ligases15, 16.

Here we describe a screen for factors controlling CMG helicase disassembly in the *C. elegans* early embryo, leading to the identification of a cullin ligase that we show is also essential for chromatin extraction of CMG during S-phase in *Xenopus* egg extracts, where we find that recruitment of the ligase to chromatin is a key regulated step during DNA replication termination. We also identify a second pathway for CMG helicase disassembly during mitosis in *C. elegans*, indicating that replisome disassembly in metazoa involves additional mechanisms not previously identified in yeast.

Results

A cytological assay for replisome dissolution in *C. elegans* early embryos

We established an *in vivo* assay for defects in replisome disassembly in live *C. elegans* early embryos (Figure 1), by time-lapse analysis of embryos simultaneously expressing mCherry-Histone H2B and GFP-tagged CMG components17, 18. We initially examined GFP-tagged versions of CDC-45 and the GINS component SLD-5, after depletion of CDC-48. As shown in Supplementary Figure 1a, both GFP-CDC-45 and GFP-SLD-5 were absent from chromatin during prophase in control embryos, but were chromatin-associated throughout mitosis in embryos treated with *cdc-48* RNAi. We also screened all the known or predicted adaptors of worm CDC-4819–21 (Supplementary Figure 1b), and found that depletion of either subunit of the NPL-4_UFD-1 heterodimer22, 23 led to persistence of both GINS and CDC-45 on condensing prophase chromatin (Figure 1b-c, Supplementary Figure 1c, Supplementary Movies 1-2). Moreover, a fraction of GFP-MCM-3 was present on chromatin during early mitosis in embryos depleted for NPL-4 or CDC-48 (Figure 1d and Supplementary Figure 1d-e, *npl-4* or *cdc-48* RNAi, ‘early metaphase’; note that the high concentration of MCM-2-7 in the nucleus precluded the examination of prophase chromatin). Finally, we used fluorescence recovery after photobleaching (FRAP) to confirm that *npl-4* RNAi caused ‘old’ CMG components to persist on chromatin after S-phase, rather

than driving the premature assembly of 'new' CMG complexes (Figure 1h, Supplementary Movie 3, Supplementary Figure 1g-h). These findings indicated that CDC-48 and its co-factors NPL-4 and UFD-1 are essential for the extraction of CMG components from chromatin during S-phase in the *C. elegans* early embryo.

Consistent with these data, we found that *npl-4* RNAi led to a strong accumulation of the CMG helicase with ubiquitylated MCM-7 subunit (Figure 1e-g). Ubiquitylation of CMG was reduced if the completion of DNA replication was inhibited (Supplementary Figure 1f), by RNAi depletion of the ribonucleotide reductase RNR-1 as described previously18, consistent with the idea that CMG ubiquitylation in the worm embryo is linked to DNA replication termination as in budding yeast and *Xenopus laevis*10, 11.

CUL-2^{LRR-1} is required for ubiquitylation and disassembly of the CMG helicase during S-phase in *C. elegans*

The *C. elegans* genome encodes CUL-1 to CUL-5 (Supplementary Figure 2a), which are orthologues of the five cullins found in diverse metazoa, plus CUL-6 that is a paralogue of CUL-124. Using our cytological assay for CMG disassembly, we found that RNAi depletion of CUL-2 was unique in causing persistence of SLD-5 and PSF-1 on prophase chromatin (Figure 2a, Supplementary Figure 2b and Supplementary Movie 4). The same defect was observed after depletion of the RING finger protein Rbx1, which links CUL-2 (and CUL-1/3/4/6) to its cognate ubiquitin conjugating enzyme, or after depletion of the worm orthologues of Elongin B and Elongin C, which connect CUL-2 (and CUL-5) to its substrate adaptors (Figure2a; see below for Elongin B). These findings indicated that a CUL-2 ligase regulates disassembly of the CMG helicase during S-phase in *C. elegans*, probably involving ubiquitin ligase activity, since not only CUL-2 but also RBX-1 is required for removing CMG from chromatin.

Six different substrate adaptors of CUL-2 have been characterized in *C. elegans* (Supplementary Figure 2c), five of which are conserved in humans. We depleted each of these and found that RNAi to *lrr-1* (Leucine-rich repeats 1) was unique in causing GINS and CDC-45 to persist on prophase chromatin (Figure 2b, Supplementary Figure 2d and Supplementary Movie 5 for GINS; see Supplementary Figure 3d below for CDC-45). Importantly, depletion of LRR-1 also dramatically reduced CMG ubiquitylation, when replisome disassembly was blocked by *npl-4* RNAi (Figure 2c-d). These data indicated that CUL-2^{LRR-1} regulates CMG disassembly during DNA replication termination in the *C. elegans* early embryo.

A mitotic pathway for CMG chromatin extraction requires the CDC-48 co-factor UBXN-3

Although CMG was initially retained on prophase chromatin following RNAi depletion of CUL-2^{LRR-1}, both GINS and CDC-45 were then released from chromatin a few minutes before nuclear envelope breakdown in late prophase (Figure 3a, Supplementary Figure 3a, b, d, and Supplementary Movies 4-5; note that MCM-2-7 could not be examined on prophase chromatin, as discussed above). Moreover, the same was true in *lrr-1Δ* / *lrr-1Δ* homozygous embryos that lack the LRR-1 protein (Figure 3c and Supplementary Figure 3c; *lrr-1* is an essential gene in *C. elegans*, but the first embryonic cell cycles in homozygous *lrr-1Δ*

embryos can be examined as described in Methods). The delayed release of CMG components from chromatin in the absence of LRR-1 was not produced by a delay in the completion of S-phase, since RNAi depletion of the catalytic or primase subunits of Pol alpha greatly extended the length of S-phase, yet did not cause CMG to persist on condensing chromatin (Figure 3a-b, *div-1* and *pol alpha* RNAi), consistent with our previous data17. Instead, these findings indicated that the *C. elegans* early embryo has two different pathways for CMG helicase disassembly (Supplementary Figure 3e). The first pathway acts during DNA replication termination and requires CUL-2^{LRR-1}, whereas the second provides backup and is activated during prophase. Consistent with the existence of the second pathway, we found that depletion of LRR-1 did not cause a strong accumulation of CMG in embryo extracts, compared to depletion of NPL-4 (Figure 3d, compare samples 2 and 3). However, *lrr-1* RNAi did abrogate the basal level of CMG ubiquitylation that is seen in control embryos (Figure 3d-e, longer exposures, compare samples 1 and 2).

Both CMG disassembly pathways require CDC-48 / UFD-1 / NPL-4, since depletion of the latter leads to persistence of CMG on chromatin throughout mitosis (Figure 1, Supplementary Figure 1). In addition to the three ‘core’ co-factors that form mutually exclusive complexes with CDC-48 / p97, namely UFD-1_NPL-4, UBXN-2 / p47 and UBXN-6 / UBXD1, eukaryotic cells also contain a range of other partners of p97 / CDC-48 that recruit the segregase to specific targets or to particular sub-cellular locations25–27 (Supplementary Figure 1b). To test whether one of these links CDC-48 to the mitotic CMG disassembly pathway, we combined *lrr-1* RNAi with depletion of each of the predicted CDC-48 adaptors in *C. elegans* (see Methods), and then examined the association of CMG components with mitotic chromatin. Amongst all the tested combinations, only simultaneous depletion of LRR-1 and UBXN-3 led to persistence of GFP-CDC-45, GFP-PSF-1 and GFP-SLD-5 on mitotic chromatin (Figure 4a, Supplementary Figure 4a-b and Supplementary Movie 6). In contrast, these CMG components were released from chromatin before prophase in embryos treated with RNAi to *ubxn-3* alone (Figure 4a, Supplementary Figure 4a-b and Supplementary Movie 7).

To assay directly the level of the CMG helicase in the presence or absence of UBXN-3, we isolated GFP-PSF-1 from embryo extracts as above. Simultaneous RNAi to *ubxn-3* and *lrr-1* led to a striking accumulation of CMG, equivalent to that seen with *npl-4* RNAi (Figure 4b, compare level of CDC-45 and MCM-2 associated with GINS in samples 2-4), with residual ubiquitylation of CMG as seen with *npl-4 lrr-1* RNAi (compare Figure 4b samples 3-4 with Figure 3d-e samples 3-4). Together with the imaging data described above, these findings identify UBXN-3 as a factor required for a mitotic pathway of CMG disassembly in the *C. elegans* early embryo.

The SUMO protease ULP-4 modulates the mitotic CMG disassembly pathway

To screen for regulators of the mitotic CMG disassembly pathway, we combined *lrr-1* RNAi with depletion of candidate proteins, including factors that regulate cell division or genome integrity (Supplementary Table 1). These included mitotic regulators such as the Aurora B and Polo kinases AIR-2 and PLK-1, candidate ubiquitin ligases such as BRC-1 (BRCA1) and SMC-5, regulators of DNA replication such as the ATL-1 checkpoint kinase, and

components of the SUMO pathway. Uniquely amongst these factors, we found that co-depletion of the SUMO protease ULP-4 with LRR-1 delayed the release of CMG components from chromatin, until at or after nuclear envelope breakdown, (Figure 4c and Supplementary Figure 4c-d). ULP-4 is the major SUMO protease during mitosis in *C. elegans*, analogous to SENP6-7 in human cells, and is present on mitotic chromosomes and at the spindle midzone 28. Although *ulp-4 lrr-1* RNAi produced a less severe CMG disassembly defect than co-depletion of LRR-1 and UBXN-3, these findings indicated that the UBXN-3-dependent mitotic pathway for CMG disassembly is also modulated by ULP-4.

Combining defects in the S-phase and mitotic CMG disassembly pathways produces synthetic lethality

Previous work showed that LRR-1 is essential for germ cell formation and embryonic development in *C. elegans*29, 30. In contrast, RNAi to *ubxn-3* or *ulp-4* is tolerated without causing severe embryonic lethality (see below), indicating that the mitotic CMG disassembly pathway is dispensable in worms that can disassemble CMG via the CUL-2^{LRR-1} S-phase pathway.

To explore the physiological importance of the mitotic CMG disassembly pathway should CUL-2^{LRR-1} fail to act, we fed worms on bacteria with 10% expressing *lrr-1* RNAi (Figure 4d shows that this low dose of lrr-1 RNAi scarcely affects viability), and then gradually increased the proportion of bacteria that expressed RNAi to *ubxn-3* or *ulp-4*. Strikingly, even the lowest tested dose of *ubxn-3* RNAi produced 100% lethality in combination with 10% *lrr-1* RNAi, despite both single RNAi treatments causing almost no detectable lethality (Figure 4e). Similarly, the lowest tested dose of *ulp-4* RNAi produced 90% embryonic lethality in combination with 10% *lrr-1* RNAi, even though neither individual RNAi treatment affected viability to a significant degree (Figure 4f). These findings indicate that both UBXN-3 and ULP-4 become essential when the function of CUL-2^{LRR-1} is even partially defective, consistent with the possibility that the mitotic CMG disassembly pathway provides an essential back up for the S-phase pathway (though this remains to be demonstrated directly in future studies).

LRR-1 couples the CUL-2^{LRR-1} ubiquitin ligase to the worm replisome

To test whether CUL-2^{LRR-1} associates with the worm replisome, we treated control and *GFP-psf-1* worms with *npl-4* RNAi to block replisome disassembly, and then used isolated embryos to generate extracts that were incubated with beads coupled to anti-GFP antibodies. A fraction of the resultant material was analysed by immunoblotting, to confirm the specific isolation of ubiquitylated CMG helicase from the *GFP-psf-1* embryos (Figure 5a). The remainder was resolved by SDS-PAGE (Figure 5b) and analysed by mass spectrometry (Supplementary Table 2).

The worm CMG helicase and associated factors showed remarkable convergence with the better-characterized replisome from budding yeast (Supplementary Table 2, Figure 5c: note that our data represent the worm replisome just after termination of DNA synthesis). Notably, CUL-2^{LRR-1} was the only cullin ligase associated with the post-termination worm replisome (Supplementary Table 2), and we subsequently found that the presence of CUL-2

Europe PMC Funders Author Manuscripts

in the purified material was dependent upon LRR-1 (Figure 5d, Supplementary Table 3). Therefore, LRR-1 is required for CUL-2 to associate with the replisome in *C. elegans* early embryos.

CUL2^{LRR1} associates with the vertebrate replisome during DNA replication termination in *Xenopus* egg extracts

In analogous experiments, we examined whether CUL2^{LRR1} associated with the vertebrate replisome during DNA replication termination in *Xenopus* egg extracts. Sperm nuclei were added to an extract supplemented with a dominant negative p97 mutant as well as the neddylation inhibitor MLN4924, both of which block CMG disassembly at the end of S-phase11. After bulk DNA replication had been completed (see below), the CMG helicase was isolated from the chromatin fraction by DNA digestion followed by immunoprecipitation of MCM3 (Figure 6a; non-specific IgG was used as a negative control). The resultant material was then analysed by mass spectrometry and found to contain orthologues of every component of the isolated post-termination worm replisome (Supplementary Table 4). Strikingly, the post-termination vertebrate replisome was associated with a single cullin ligase, namely CUL2^{LRR1} (Supplementary Table 4, Figure 6b). Correspondingly, immunoprecipitation of LRR1 from digested chromatin, after inhibition of replisome disassembly with a p97 inhibitor, led to co-purification not only of CUL2 and Elongin B/C, but also of the frog replisome (Figure 6c, Supplementary Table 5). Interestingly, immunoprecipitation of LRR1 from digested chromatin under such conditions led to co-depletion of CUL2 (Supplementary Figure 5a, compare flowthrough for IgG and LRR1 IPs). Therefore, these data not only demonstrate that the association of CUL2^{LRR1} with the replisome is conserved from worms to vertebrates, but also indicate that CUL2^{LRR1} is the major CUL2 ligase on interphase chromatin.

The recruitment of *Xenopus* CUL2^{LRR1} to chromatin was dependent upon replisome assembly during the initiation of chromosome replication (Figure 6d). Moreover, the association of CUL2^{LRR1} with chromatin was greatly increased when replisome disassembly at the end of S-phase was blocked by addition of MLN4924 to the extracts (Figure 6e: Figure 6f and Supplementary Figure 5b show that replication kinetics were not affected by MLN4924, consistent with our previous findings11). These data suggested that regulated recruitment of CUL2^{LRR1} to chromatin is an important feature of the mechanism of replisome disassembly during DNA replication termination. Correspondingly, CUL2^{LRR1} was not recruited to chromatin if DNA synthesis and subsequent termination were blocked, by addition of the DNA polymerase inhibitor aphidicolin (Figure 6g; note that caffeine had to be added to these reactions, to prevent the S-phase checkpoint pathway from limiting the accumulation of CMG on chromatin, by blocking new initiation events).

To test directly whether chromatin recruitment of CUL2^{LRR1} was linked to DNA replication termination, we either inhibited replisome disassembly after termination of DNA synthesis, by inactivating CDC48 / p97 with the small molecule inhibitor NMS87331, 32, or delayed the convergence of DNA replication forks during termination, by addition of the TOPO2 inhibitor ICRF19311, 33. Neither treatment affected the kinetics of bulk DNA synthesis (Supplementary Figure 5c), consistent with previous studies9, 11. Inhibition of p97 / CDC48

with NMS873 caused a dramatic accumulation of CMG and $CUL2^{LRR1}$ on chromatin (Figure 6h, NMS873). However, delaying DNA replication fork convergence with ICRF193 delayed removal of CMG components from chromatin (Figure 6h, compare CDC45 and PSF2 between control and ICRF193 treatment), but this was not associated with chromatin recruitment of $CUL2^{LRR1}$ (Figure 6h). These findings indicate that $CUL2^{LRR1}$ only associates with the replisome during the termination of DNA replication.

Active $CUL2^{LRR1}$ is essential for extraction of the CMG helicase from chromatin at the end of chromosome replication in *Xenopus* egg extracts

Depletion of frog egg extracts with antibodies to CUL2-RBX1 (Figure 7a) abolished detectable chromatin recruitment of $CUL2^{LRR1}$ during DNA replication termination (Figure 7b), even in the presence of MLN4924 that stabilises the association of the ligase with the post-termination replisome as shown above. The kinetics of bulk DNA replication in egg extracts were not affected by CUL2 depletion (Figure 7d-e), but the release of CMG components from chromatin at the end of replication was inhibited (Figure 7f). Moreover, ubiquitylation of the MCM7 subunit of CMG was both delayed and greatly reduced under such conditions (Figure 7f, MCM7).

To confirm that the failure of CMG chromatin extraction was indeed due to inactivation of CUL2-RBX1, we attempted to rescue the defect by addition of recombinant CUL2-RBX1, purified from insect cells. However, we noted that LRR1 was co-depleted from extracts along with CUL2 (Figure 7c), and thus we performed the rescue experiments in the presence or absence of recombinant LRR1, expressed and purified from *E. coli*. By isolating sperm chromatin from *Xenopus* egg extracts after the completion of bulk DNA replication, we confirmed that CMG components were absent from chromatin in mock-depleted extracts that were subjected to two rounds of immunoprecipitation with rabbit IgG (Figure 7g, lane 1), whereas CMG remained on chromatin following depletion of $CUL2^{LRR1}$ (Figure 7g, lane 2), as shown above (Figure 7f). Crucially, the defect in CMG helicase disassembly was not rescued by addition of CUL2-RBX1 complex alone (Figure 7g, lane 3), but was fully complemented by the addition of CUL2-RBX1 together with recombinant LRR1 (Figure 7g, lane 5).

To explore whether the E3 ligase activity of $CUL2^{LRR1}$ was required for CMG chromatin extraction, we tested a version of CUL2-RBX1 with a mutated neddylation site and another mutation in the interaction site with the DCN1 neddylase34, since neddylation promotes cullin function in vertebrates and we previously showed that the neddylation inhibitor MLN4924 blocks CMG ubiquitylation and chromatin extraction during DNA replication termination in *Xenopus* egg extracts11. Importantly, mutated CUL2-RBX1 was not able to restore CMG chromatin extraction in CUL2-depleted extracts (Figure 7g, lane 4), even when added with recombinant LRR1 (Figure 7g, lane 6).

These findings demonstrate that CMG helicase disassembly at the end of chromosome replication in *Xenopus* egg extracts requires LRR1 and neddylation of CUL2, indicating a requirement for active $CUL2^{LRR1}$. Together with past work establishing CMG helicase disassembly as the final regulated step during chromosome replication in vertebrates9, these findings establish the ubiquitin ligase $CUL2^{LRR1}$ as the key enzyme in this process.

Discussion

Previous work showed that LRR-1 is essential for germ cell formation and embryonic development in *C. elegans*29, 30. Inactivation of *lrr-1* induces DNA damage, thereby blocking germ cell proliferation and delaying mitotic entry in the early embryo29, via the ATL-1 S-phase checkpoint pathway that is equivalent to the ATR response in vertebrates. The molecular basis for DNA damage induction in the absence of LRR-1 is poorly understood, but a recent study found that low-dose RNAi to CMG components could suppress the sterility phenotype of *lrr-1Δ* worms, as well as suppressing the embryonic lethality associated with a *cul-2* temperature sensitive allele under semi-restrictive conditions35. These findings suggest that the CMG helicase is a functionally important target of CUL-2^{LRR-1} in *C. elegans*.

Our data indicate that $CUL2^{LRR1}$ activity is required to extract CMG from chromatin during DNA replication termination, both in worms and in frog egg extracts, indicating that the role of $CUL2^{LRR1}$ in the S-phase pathway of CMG helicase disassembly is widely conserved in metazoa. Moreover, our data identify chromatin recruitment of $CUL2^{LRR1}$ as a key regulated step (Figure 6).

Despite metazoa and yeast using different cullin ligases to trigger replisome disassembly during termination of replication, our data highlight invariant features of the disassembly mechanism in diverse eukaryotes. Firstly, the CMG helicase is ubiquitylated on its MCM7 subunit at the end of chromosome replication in budding yeast10, worm (this study) and frog9, 11, perhaps linked to a structural change in the CMG helicase that renders it accessible to the E3 ligase during DNA replication termination. Secondly, we found that UFD-1 and NPL-4 are required for CDC-48-dependent disassembly of the CMG helicase during S-phase in *C. elegans* (Figure 1 and Supplementary 1), and UFD1-NPL4 associate with the 'post-termination' replisome in *Xenopus* (Supplementary Table 4), consistent with previous data36. These findings indicate that UFD1 and NPL4 mediate CDC48-dependent replisome disassembly in metazoa, and we predict that the same is true for budding yeast.

Whereas budding yeast appears to have a single pathway for CMG helicase disassembly that acts during S-phase10, our *C. elegans* data indicate that metazoa have an additional CMG disassembly mechanism that operates during mitosis and requires the UBXN-3 partner of CDC-48. Interestingly, a recent study found that depletion of UBXN-3 sensitises worm embryos to DNA replication inhibitors, consistent with a role for UBXN-3 in regulation of the replisome37. It remains to be determined in future studies whether the mitotic pathway is also controlled by an E3 ubiquitin ligase, analogous to the role of CUL-2^{LRR-1} during S-phase, but we have found that the mitotic CMG disassembly pathway is modulated by the ULP-4 SUMO protease, which is the major desumoylase on mitotic chromosomes28. It will thus be interesting to explore whether SUMO regulates CMG helicase disassembly during mitosis, perhaps inhibiting disassembly until desumoyation by ULP-4, or whether ULP-4 acts in some other way, for example by recruiting CDC-48 partners like UBXN-3 to mitotic chromatin.

We have found that UBXN-3 and ULP-4 become essential for viability when the function of LRR-1 is even partially compromised (Figure 4), highlighting the physiological importance of UBXN-3 and ULP-4. These findings suggest that the mitotic CMG disassembly pathway provides important backup to the DNA replication termination pathway, although at present we cannot exclude that our data also reflect other roles for LRR-1, UBXN-3 and ULP-4. Interestingly, the human FAF1 protein is orthologous to UBXN-3, associates with p97-UFD1-NPL438 and is deleted or depleted in many human cancers39. Moreover, depletion of FAF1 in human cells leads to defective progression and increased stalling of DNA replication forks37. Should it be possible in the future to develop small molecule inhibitors of $CUL2^{LRR1}$, our data indicate that transient or partial inhibition of the $CUL2^{LRR1}$ E3 ligase might cause synthetic lethality in cancer cells with defective FAF1. It is thus to be hoped that a deeper understanding of the biology of replisome disassembly during DNA replication termination will have important implications for human pathology.

Methods

C. elegans modification and maintenance

The *C. elegans* strains used in this study were derived from the 'Bristol N2' wild type. Worms were maintained according to standard procedures 43 and were grown on 'Nematode Growth Medium' (NGM: 3 g/l NaCl; 2.5 g/l peptone; 20 g/l agar; 5 mg/l cholesterol; 1 mM $CaCl_2$; 1 mM $MgSO_4$; 2.7 g/l KH_2PO_4; 0.89 g/l K_2HPO_4). The following strains were used:

TG1753: *unc-119(ed3) III; gtIs64[pie-1p::gfp::mcm-3 + unc-119(+)]; ltIs37[pie-1p::mCherry::his-58+ unc-119(+)]*

TG1754: *unc-119(ed3) III; gtIs65[pie-1p::gfp::cdc-45 + unc-119(+)]; ltIs37*

TG1756: *unc-119(ed3) III; gtIs67[pie-1p::gfp::sld-5 + unc-119(+)]; ltIs37*

KAL1: *psf-1(lab1[gfp::TEV::S-tag::psf-1 + loxP unc-119(+) loxP])*

KAL2: *mcm-7(lab2[mcm-7::5xHis::9xFlag + loxP unc-119(+) loxP])*

KAL3: *psf-1(lab1); ltIs37*

KAL4: *psf-1(lab1); mcm-7(lab2)*

WLP145: *lrr-1(tm3543)/mIn1 II*; *ruIs32 III*

KAL5: *psf-1(lab1) lrr-1(tm3543)/mIn1 II.*

The KAL1 and KAL2 strains were generated using the CRISPR/CAS9 system (Knudra transgenics, USA) and were then out-crossed eight times with the N2 wild type. KAL3 was derived from a cross of KAL1 with TG1753, KAL4 was made by crossing KAL1 with KAL2, and KAL5 was generated by crossing KAL1 to WLP145.

The *lrr-1(tm3543)* allele contains a 488bp deletion within the open reading frame, resulting in a frame shift closely followed by a premature stop codon, so that *lrr-1 (tm3543)*

approximates a null allele for *lrr-1*29. The WLP145 strain contains the *mIn1* balancer chromosome that supplies LRR-1 function and thus preserves viability. The *mIn1* balancer also expresses GFP and so can be selected against by microscopic examination44, thereby facilitating the isolation of homozygous *lrr-1(tm3543)* worms. The latter do not produce embryos due to defects in germ cell proliferation, but fertility can be restored by knocking down the *atl-1* gene that encodes the worm orthologue of ATR, producing homozygous *lrr-1(tm3543)* embryos that facilitate the analysis of the first embryonic cell cycles, but that do not develop fully to produce viable worms29.

RNA interference

RNAi was performed by feeding worms with bacteria containing plasmids that express double-stranded RNA45. For microscopy experiments, worms were fed on 6cm plates containing the following medium: 3 g/l NaCl, 20 g/l agarose, 5 mg/l cholesterol, 1 mM $CaCl_2$, 1 mM $MgSO_4$, 2.7 g/l KH_2PO_4, 0.89 g/l K_2HPO_4, 1 mM IPTG and 100 mg/l Ampicillin. For immunoprecipitation experiments, worms were fed on 15cm plates containing NGM medium supplemented with 1 mM IPTG and 100 mg/l Ampicillin,

The plasmids expressing dsRNA were either derived from a commercial RNAi library (SourceBioscience, UK; *cdc-48.1*, *cdc-48.2*, *ufd-1*, *cul-1*, *cul-3*, *cul-4*, *cul-5*, *cul-6*, *rbx-1*, *vhl-1*, *zyg-11*, *fem-1*, *zer-1*, *zif-1* and *brd-1*), or else were made by cloning PCR products into the vector L444045. In the latter case, we either amplified 1kb products from cDNA (*npl-4.2*, *mcm-3 3'UTR*, *cul-2*, *elc-1*, *elb-1*, *lrr-1*, *atl-1*, *ubxn-3, air-2, plk-1, cyb-3, cya-1, gsk-3, mbk-2, brc-1, D2085.4, smc-5, nse-1, C32D5.10, C32D5.11, eel-1, Y47G6A.31, spat-3, mig-32, rnf-113, vps-11, T01G5.7, atl-1, atm-1, smc-4, pif-1, dvc-1, smo-1, ubc-9 and ulp-4*), or amplified full-length cDNA for open reading frames shorter than 1kb, using a cDNA library that was a gift from Bettina Meyer. The *mcm-3 3'UTR* was amplified from genomic DNA. Details of sequences used in RNAi vectors are provided in Supplementary Table 8.

To target more than one gene simultaneously by RNAi, we either fed an equal mixture of bacteria expressing the corresponding dsRNA (*cdc-48.1* and *cdc-48.2,* or *cul-1* and *cul-6*), or else cloned contiguous 1kb fragments for each gene into a single L4440 plasmid (all other experiments).

When screening the set of CDC-48 co-factors by RNAi, we either targeted single genes (*ubxn-2*, *vms-1*, *atx-3*, *cyh-1*, *aip-1*, *ufd-3* and *ufd-2*), or else generated L4440-derived vectors containing contiguous combinations of DNA fragments to target multiple genes simultaneously (*ubxn-1* + *ubxn-4*, *ubxn-3* + H40L08.1 + *ubc-23*, *ubxn-5* + H40L08.1, *ubxn-6* + B0024.10, *ubxn-1* + *ubxn-2* + *ubxn-3*, *hrdl-1* + *sel-11* + Y119C1B.5 and *cup-2* + R151.6). Combinations perturbing CMG disassembly were then deconvolved using the corresponding single RNAi vectors. An empty L4440 plasmid was used as control for RNAi experiments throughout this study.

Microscopy

Worms at the larval L4 stage were incubated on 6 cm RNAi feeding plates for 28-34 hours at 25°C, or for 48-52 hours at 20°C when using the GFP-PSF-1 knock-in worms. Adult worms

were then dissected in M9 medium (6 g/l Na_2HPO_4, 3 g/l KH_2PO_4, 5 g/l NaCl, 0.25 g/l $MgSO_4$) and embryos were mounted on a 2% agarose pad. Time lapse images were then recorded as described previously17, 18, at 23–24°C using an Olympus IX81 microscope (MAG Biosystems) with a CSU-X1 spinning-disk confocal imager (Yokogawa Electric Corporation), a Cascade II camera (Photometrics) and a 60X/1.40 Plan Apochromat oil immersion lens (Olympus). A single optical section (z-layer) was imaged for each time point. Photobleaching of the female pronucleus in the first embryonic cell cycle was done with a 488nm laser using the 'iLas2 system' (Roger Scientific).

Images were captured using MetaMorph software (Molecular Devices) and analysed with ImageJ software (National Institutes of Health). For each timelapse experiment depicted in the figures, the raw images for selected timepoints were rotated in order to orient the anterior of the chosen embryo to the left, and then cropped to focus on a particular nucleus or nuclei, or on the entire embryo. The series of images were then combined into a contiguous sequence, and the images were subjected to Gaussian Blur with a radius of 1 pixel. Subsequently, the levels were adjusted, the pixel density was adjusted to 300 dots per inch and the bit depth was changed from 16-bits to 8-bits per channel. Images were processed in a similar manner in order to generate videos, except that timepoints were not combined into a sequence and the pixel density was not adjusted to 300 dpi.

To generate the data in Figure 3b, the duration of cell cycle phases in the second cell cycle (P1 cell) were measured as follows. Interphase was measured from nuclear formation (appearance of nuclear GFP-PSF-1) until the start of chromosome condensation, which marked the beginning of prophase. The latter phase ended with nuclear envelope breakdown, after which the time of metaphase and anaphase was measured as the period until nuclear envelop reformation.

Synthetic lethality in *C. elegans*

For the experiment in Figure 4, the RNAi dose was titrated by mixing the indicated proportion of bacterial cultures expressing *lrr-1*, *ubxn-3* and *ulp-4* double-stranded RNA, or containing an empty plasmid. All cultures were grown to OD600 = 1, and worms were then incubated on RNAi feeding plates for 48 hours at 20°C. For each condition, triplicate experiments were performed, in each of which 5 adult worms were allowed to produce embryos on a plate during a period of 150 minutes, after which the adults were removed and the embryos were counted. Two days later, the number of embryos that had developed into viable adults was determined (between 69 and 94 embryos for each set of embryos from 5 worms). Embryonic viability was expressed as the ratio between the number of viable embryos and the total number of embryos, and the average and standard deviation were then determined for each triplicate set.

Extracts of worm embryos and immunoprecipitation of protein complexes

RNAse III-deficient HT115 bacteria were transformed with an L4440-derived plasmid, corresponding to the required RNAi treatment. A 0.5ml pre-culture was then grown overnight, and used to inoculate a 400 ml culture in 'Terrific Broth' (12 g/l Tryptone, 24 g/l yeast extract, 9.4 g/l K2HPO4, 2.2 g/l KH2PO4, adjusted to pH 7). After 7 hours of growth

in a baffled flask at 37°C with agitation, expression of dsRNA was induced overnight at 20°C by addition of 3mM IPTG. The bacteria were then pelleted and resuspended with one-fifth volume of buffer (M9 medium supplemented with 75 mg/l cholesterol; 100 mg/l ampicillin; 50 mg/l tetracycline; 12.5 mg/l amphotericin B; 3 mM IPTG).

For each experiment, 1ml of a synchronized population of L4 worms expressing GFP-PSF-1 were fed for 50 hours at 20°C on a 15 cm RNAi plate (see above), supplemented with 8 g of bacterial pellet for the required RNAi treatment, prepared as described above. After feeding, the adults worms were washed in M9 medium and resuspended for 2 minutes at room temperature in 14 ml of 'bleaching solution' (for 100 ml: 36.5 ml H_2O, 45.5 ml 2N NaOH and 18 ml ClNaO 4%), then pelleted for 1 minute at 300 g. This bleaching procedure was repeated two more times, corresponding to a total of 8-12 minutes in bleaching solution, in order to lyse the adult worms and release embryos (about 0.6-0.8 g). After bleaching, the embryos were washed twice with M9 medium.

The remaining steps were performed at 4°C and are based on our previously described methods for isolating protein complexes from yeast cells 1, 10. Embryos were washed twice with lysis buffer (100 mM HEPES-KOH pH 7.9, 50 mM potassium acetate, 10 mM magnesium acetate, 2 mM EDTA), and then resuspended with three volumes of lysis buffer that was supplemented with 2 mM sodium fluoride, 2 mM sodium β-glycerophosphate pentahydrate, 1 mM dithiothreitol (DTT), 1% Protease Inhibitor Cocktail (P8215, Sigma-Aldrich), and 1X 'Complete Protease Inhibitor Cocktail' (05056489001, Roche; one tablet dissolved in 1 ml water makes a 25× stock solution). The mixture was transferred drop-wise into liquid nitrogen to prepare 'popcorn', which was stored at -80°C. We then ground ~2.5 g of the frozen popcorn in a SPEX SamplePrep 6780 Freezer/Mill. After thawing, we added one-quarter volume of 'glycerol mix' buffer (lysis buffer supplemented with 50% glycerol, 300 mM potassium acetate, 0.5% detergent IGEPAL CA-630, protease inhibitors, and DTT at the concentrations mentioned above). De-ubiquitylase enzymes were inhibited by addition of 5μM Ubiquitin PrG (prepared by Axel Knebel and Clare Johnson, MRC PPU, Dundee), and chromosomal DNA was digested with 1600 U of Pierce Universal Nuclease (123991963, Fisher) for 30 minutes at 4°C. Extracts were centrifuged at 25000 g for 30 minutes and then for 100000 g for 1 hour, before pre-incubation with agarose beads (0.4 ml slurry) for 45 minutes. At this point, 50 μl of extract was added to 100 μl of 1.5X Laemmli buffer and stored at -80°C. The remainder of the extracts were then incubated for 90 minutes with 40 μl of GFP-Trap_A beads (Chromotek). The beads were washed four times with 1 ml of wash buffer (100 mM HEPES-KOH pH 7.9, 100 mM potassium acetate, 10 mM magnesium acetate, 2 mM EDTA, 0.1% IGEPAL CA-630, 2 mM sodium fluoride, 2 mM sodium β-glycerophosphate pentahydrate, plus protease inhibitors as above) and bound proteins were eluted at 95°C for 5 min in 100 μl of 1x Laemmli buffer (or 50 μl when used for mass spectrometry analysis) and stored at -80°C.

Chromatin isolation from *Xenopus* egg extracts

Chromatin assembled in *Xenopus* egg extract was isolated in ANIB/100 buffer as described before46. A sample without added sperm DNA was processed in an analogous way to provide a chromatin specificity control.

Isolation of CMG helicase or LRR1 from *Xenopus* chromatin

To isolated *Xenopus* CMG (Figure 6), interphase egg extract was supplemented with 10-15 ng/μl demembranated sperm DNA and treated with caffeine, p97D1D2 mutant and 10μM MLN4924. Chromatin from 3.75 ml of extract was isolated in late S-phase in ANIB/100 buffer supplemented with 10 mM 2-chloroacetamide (Millipore), and chromosomal DNA was then digested with Benzonase nuclease as described before47. The resulting protein complexes were incubated with 225μl of magnetic beads (Dynabeads M-270 Epoxy, Invitrogen) covalently coupled to either affinity-purified sheep Mcm3 antibody or IgG from sheep serum (I5131, Sigma), and the immunoprecipitated material was analysed by mass spectrometry as described previously47.

LRR1 was isolated from digested chromatin in an analogous manner, except that replisome disassembly was blocked by addition of 50μM NMS873 (Figure 6c) or MLN4924 (Supplementary Table 5). Chromatin samples isolated from 1.9 ml (Figure 6c) or 100 μl (Supplementary Table 5) of egg extract were incubated with 225μl (Figure 6c) or 50μl (Supplementary Table 5) of Dynabeads Protein G (10004D, Life Technologies) cross-linked (BS3, ABE5976, Source Bioscience) to 45 μg or 10 μg respectively of affinity-purified sheep LRR1 antibodies, or IgG from sheep serum (I5131, Sigma), according to the manufacturer's instructions. After two hours incubation with rotation at 4°C, the beads were washed twice with LFB1/50 buffer (40 mM Hepes/KOH pH 8.0, 20 mM potassium phosphate pH 8.0, 50 mM potassium chloride, 2 mM magnesium chloride, 1 mM EGTA; 10% sucrose w/v; 2 mM DTT; 1 μg/ml aprotinin; 1 μg/ml leupeptin; 1 μg/ml pepstatin), once with LFB1/50 supplemented with 0.1% triton X-100, and again twice with LFB1/50 buffer alone. The immunoprecipitated proteins were eluted by boiling in 2x NuPAGE LDS loading buffer (Life Technologies).

Immunodepletion of CUL2 from egg extracts and rescue with recombinant proteins

Cullin2 immunodepletions were performed using Dynabeads Protein A (life technologies, 10002D) coupled to antibodies against a complex of human CUL2-RBX1 (Supplementary Figure 6 shows that mammalian CUL2 is nearly identical to Xenopus CUL2). Depletion of 200 μl of extract required 2 rounds of 1 hour incubation at 4° with 100 μl of beads coupled to 42 μg of anti-CUL2-RBX1 (RA0333). Mock-depleted controls were performed in parallel using beads coupled to an equivalent amount of rabbit IgG. For rescue experiments, recombinant wild type Hs_CUL2-RBX1 or mutant Hs_CUL2-RBX1 (with the CUL2 mutations K689R in the neddylation site and K719R mutation in a key contact site with the DCN1 neddylase34) were added to CUL2-immunodepleted extracts, to a final concentration of 0.2 mg/ml when added alone, or 0.1 mg/ml when added with recombinant Xl_LRR1 (the latter was added to a final concentration of 0.026 mg/ml).

Monitoring DNA synthesis in *Xenopus* egg extracts

The synthesis of nascent DNA was monitored by quantification of α^{32}P-dATP incorporation in one of two ways, as described previously46. Firstly, 16.5nM α^{32}P-dATP was added from

the start of the experiment, so that total incorporation could be monitored at each time point, by isolation of total DNA and quantification of the α^{32}P-dATP signal. Secondly, Yμ M α^{32}P-dATP was added at the indicated time points for a short pulse of 2 minutes (normal extracts) or 3 minutes (immunodepleted extracts), in order to monitor ongoing DNA synthesis at different stages of the reaction.

Immunoblotting

Samples were resolved by SDS-polyacrylamide gel electrophoresis using NuPAGE Novex 4-12% Midi Bis-Tris gels (NP0301, Life Technologies) with NuPAGE MOPS SDS buffer (NP000102, Life Technologies). To improve the resolution of ubiquitylated forms of *C. elegans* MCM-7, we used NuPAGE Novex 3-8% Tris-Acetate Midi gels (WG1602, Life Technologies) with NuPAGE Tris-Acetate SDS buffer (LA0041, Life Technologies). Proteins were transferred onto nitrocellulose membrane using the 'iBlot' Dry Transfer System (Life Technologies). Sheep or rabbit polyclonal antibodies recognizing the indicated *C. elegans* CMG components were produced for this study by the 'Division of Signal Transduction Therapy' of the MRC PPU, at the University of Dundee (S750D anti-MCM-2, S797D anti-MCM7, S782D anti-CDC-45, S789D anti-PSF-1, R3632 anti-PSF-3; Figure 5a provides validation of the specificity of S789D anti-PSF-1 and Figure S7 provides validation for the other new antibodies). The antigens for MCM-7, MCM-2 and CDC-45 corresponded to first 222 amino acids of each protein, whereas full-length protein was used for PSF-1 and PSF-3. Polyubiquitin chains were detected using mouse FK2 antibody (BML-PW8810, Enzo Life Sciences).

The following commercial antibodies were used to detect *Xenopus* proteins: monoclonal anti-PCNA (P8825, Sigma), monoclonal anti-MCM2 (BM28, BD Transduction Laboratories), monoclonal anti-CUL2 (EPR3104(2), Abcam). In addition, we used previously characterised polyclonal antibodies to detect MCM3, MCM7, CDC45 and PSF247–49. New antibodies against full-length X.l. LRR1, and a complex of human CUL2-RBX1, were raised in sheep and affinity purified (MRC PPU reagents, https://mrcppureagents.dundee.ac.uk; S962D for LRR1, validated by immunoprecipitation of *Xenopus* LRR1 and mass spectrometry as shown in Supplementary Table 5; RA0333 and SA0206 for anti-CUL2-RBX1, validated by immunoprecipitation of *Xenopus* CUL2 and immunoblotting with monoclonal anti-CUL2 EPR3104(2) from Abcam).

Conjugates to horseradish peroxidase of anti-sheep IgG from donkey (Sigma, A3415), anti-rabbit IgG from rabbit (Fisher, GZNA93401ML), or anti-mouse IgG from horse (PI-2000 Vector Labs) were used as secondary antibodies before the detection of chemoluminescent signals on Hyperfilm ECL (Amersham, GE Healthcare) using the ECL Western Blotting Detection Reagent (GE Healthcare). Antibody dilutions are provided in Supplementary Table 7.

Inhibitors for use in *Xenopus* egg extracts

The MLN4924 inhibitor of the E1 enzyme for neddylation (A01139, Active Biochem) was dissolved in DMSO at 20 mM and used at 10 μM. The DNA polymerase inhibitor aphidicolin (A0781, Sigma) was dissolved in DMSO at 10 mM and used at 40 μM. Caffeine

(C8960, Sigma) was dissolved at 100 mM in water and used at 5 mM. The p97 inhibitor NMS873 (17674, Cayman Chemical Company) was dissolved in DMSO at 10 mM and used at 50 μM. The TOPO2 inhibitor ICRF193 (Scientific Lab Supplies, 14659) was dissolved at 10 mM in DMSO and used at 20 μM.

Recombinant proteins

Recombinant p97D1D2 mutant (E305Q, E578Q) was expressed and purified from *E.coli* as before50. Recombinant p27(KIP1) was described previously51 and used at 100 nM, while geminin^{DEL} was a kind gift from Julian Blow's laboratory52. *Xenopus laevis* LRR1 was expressed in *E. coli* and purified as a SUMO-His fusion (MRC PPU reagents, University of Dundee). Wild type and mutant Hs_CUL2-RBX1 complexes were expressed in insect cells using the Dual FastBac vector (Thermo Fisher), and purified via an N-terminal Dac-TEV-tag53 on CUL2, followed by TEV cleavage and size-exclusion chromatography over a Superdex 200 HR16/60 column.

Mass spectrometry

Purified samples from worm embryos were generated as above and eluted in 50 μl Laemmli buffer, of which 30μl was resolved by SDS-polyacrylamide gel electrophoresis using NuPAGE Novex 4-12% Midi Bis-Tris gels (NP0321, Life Technologies) with NuPAGE MOPS SDS buffer (NP000102, Life Technologies). The gels were stained with 'SimplyBlue SafeStrain' colloidal coomassie (LC6060, Invitrogen), and each lane was cut into 40 slices that were then digested with trypsin and processed for mass spectrometry (MS Bioworks, USA). The data were analysed using Scaffold software (Proteome Software Inc, USA). Mass spectrometry analysis of material from frog chromatin was similar, except that samples were separated for 2 cm in a NuPAGE Novex 4-12% Mini Bis-Tris gels (NP0321, Life Technologies), which was then cut into 10 slices and analysed as above.

Cell line usage

No cell lines were used in this study.

Statistics and Reproducibility

The experiments were not randomized, no statistical method was used to predetermine sample size, and the investigators were not blinded to allocation during experiments and outcome assessment.

For microscopy experiments, at least five embryos were analysed and seen to behave similarly. For immunoblotting data, the corresponding experiments were performed the following number of times: Figure 1e (1X), Figure 1f (1X), Figure 1g (1X), Figure 2c (1X), Figure 2d (1X), Figure 3d (1X), Figure 3e (1X), Figure 4b (1X), Figure 5a (1X), Figure 5b (1X), Figure 5d (1X), Figure 6b (1X), Figure 6c (1X), Figure 7b (3X), Figure 6f (1X), Figure 6g (5X), Figure 7f (3X), Figure 7c (3X), Figure 7g (2X), Supplementary Figure 1f (1X), Supplementary Figure 5a (2X), Supplementary Table 4 (3X), Supplementary Table 5 (2X).

Other experiments were performed the following number of times: Figure 3b (1X), Figure 4d (1X), Figure 4c (3X), Figure 4d (3X), Figure 6d (3X), Figure 6e (3X), Figure 7b (1X), Figure 7d (3X), Supplementary Figure 5b (4X), Supplementary Table 2 (1X), Supplementary Table 3 (1X), Supplementary Table 4 (1X), Supplementary Table 5 (1X).

Supplementary Material

Refer to Web version on PubMed Central for supplementary material.

Acknowledgements

We gratefully acknowledge the support of the Medical Research Council (core grant MC_UU_12016/13 for KL; award MR/K007106/1 to Agnieszka Gambus) the Wellcome Trust (reference 102943/Z/13/Z for award to KL; reference 0909444/Z/09/Z for award to Anton Gartner) and the Lister Institute (award to Agnieszka Gambus) for funding our work. We thank Julian Blow for Geminin protein, MRC PPU reagents (https://mrcppureagents.dundee.ac.uk) for recombinant frog LRR1 and for producing antibodies, and Tom Deegan for helpful comments on the manuscript. We also thank Lionel Pintard for providing the worm line heterozygous for *lrr-1Δ*, Chris Ponting for advice regarding orthologues of the budding yeast Dia2 protein and Johannes Walter and Emily Low for discussing unpublished findings.

References

1. Gambus A, et al. GINS maintains association of Cdc45 with MCM in replisome progression complexes at eukaryotic DNA replication forks. Nat Cell Biol. 2006; 8:358–366. [PubMed: 16531994]
2. Moyer SE, Lewis PW, Botchan MR. Isolation of the Cdc45/Mcm2-7/GINS (CMG) complex, a candidate for the eukaryotic DNA replication fork helicase. Proc Natl Acad Sci U S A. 2006
3. Bell SP, Labib K. Chromosome Duplication in Saccharomyces cerevisiae. Genetics. 2016; 203:1027–1067. [PubMed: 27384026]
4. Deegan TD, Diffley JF. MCM: one ring to rule them all. Curr Opin Struct Biol. 2016; 37:145–151. [PubMed: 26866665]
5. O'Donnell M, Li H. The Eukaryotic Replisome Goes Under the Microscope. Curr Biol. 2016; 26:R247–256. [PubMed: 27003891]
6. Labib K, Tercero JA, Diffley JFX. Uninterrupted MCM2-7 function required for DNA replication fork progression. Science. 2000; 288:1643–1647. [PubMed: 10834843]
7. Ilves I, Petojevic T, Pesavento JJ, Botchan MR. Activation of the MCM2-7 helicase by association with Cdc45 and GINS proteins. Molecular cell. 2010; 37:247–258. [PubMed: 20122406]
8. Bell SP. DNA Replication. Terminating the replisome. Science. 2014; 346:418–419. [PubMed: 25342784]
9. Dewar JM, Budzowska M, Walter JC. The mechanism of DNA replication termination in vertebrates. Nature. 2015; 525:345–350. [PubMed: 26322582]
10. Maric M, Maculins T, De Piccoli G, Labib K. Cdc48 and a ubiquitin ligase drive disassembly of the CMG helicase at the end of DNA replication. Science. 2014; 346:1253596. [PubMed: 25342810]
11. Moreno SP, Bailey R, Campion N, Herron S, Gambus A. Polyubiquitylation drives replisome disassembly at the termination of DNA replication. Science. 2014; 346:477–481. [PubMed: 25342805]
12. Maculins T, Nkosi PJ, Nishikawa H, Labib K. Tethering of SCF(Dia2) to the Replisome Promotes Efficient Ubiquitylation and Disassembly of the CMG Helicase. Curr Biol. 2015; 25:2254–2259. [PubMed: 26255844]
13. Morohashi H, Maculins T, Labib K. The amino-terminal TPR domain of Dia2 tethers SCF(Dia2) to the replisome progression complex. Curr Biol. 2009; 19:1943–1949. [PubMed: 19913425]
14. Soucy TA, et al. An inhibitor of NEDD8-activating enzyme as a new approach to treat cancer. Nature. 2009; 458:732–736. [PubMed: 19360080]

15. Duda DM, et al. Structural insights into NEDD8 activation of cullin-RING ligases: conformational control of conjugation. Cell. 2008; 134:995–1006. [PubMed: 18805092]
16. Saha A, Deshaies RJ. Multimodal activation of the ubiquitin ligase SCF by Nedd8 conjugation. Molecular cell. 2008; 32:21–31. [PubMed: 18851830]
17. Sonneville R, Querenet M, Craig A, Gartner A, Blow JJ. The dynamics of replication licensing in live Caenorhabditis elegans embryos. J Cell Biol. 2012; 196:233–246. [PubMed: 22249291]
18. Sonneville R, Craig G, Labib K, Gartner A, Blow JJ. Both Chromosome Decondensation and Condensation Are Dependent on DNA Replication in C. elegans Embryos. Cell Rep. 2015; 12:405–417. [PubMed: 26166571]
19. Avci D, Lemberg MK. Clipping or Extracting: Two Ways to Membrane Protein Degradation. Trends Cell Biol. 2015; 25:611–622. [PubMed: 26410407]
20. Franz A, Ackermann L, Hoppe T. Ring of Change: CDC48/p97 Drives Protein Dynamics at Chromatin. Front Genet. 2016; 7:73. [PubMed: 27200082]
21. Ramadan K, Halder S, Wiseman K, Vaz B. Strategic role of the ubiquitin-dependent segregase p97 (VCP or Cdc48) in DNA replication. Chromosoma. 2016
22. Meyer HH, Shorter JG, Seemann J, Pappin D, Warren G. A complex of mammalian ufd1 and npl4 links the AAA-ATPase, p97, to ubiquitin and nuclear transport pathways. The EMBO journal. 2000; 19:2181–2192. [PubMed: 10811609]
23. Mouysset J, Kahler C, Hoppe T. A conserved role of Caenorhabditis elegans CDC-48 in ER-associated protein degradation. Journal of structural biology. 2006; 156:41–49. [PubMed: 16647269]
24. Sarikas A, Hartmann T, Pan ZQ. The cullin protein family. Genome Biol. 2011; 12:220. [PubMed: 21554755]
25. Kloppsteck P, Ewens CA, Forster A, Zhang X, Freemont PS. Regulation of p97 in the ubiquitin-proteasome system by the UBX protein-family. Biochim Biophys Acta. 2012; 1823:125–129. [PubMed: 21963883]
26. Meyer H, Bug M, Bremer S. Emerging functions of the VCP/p97 AAA-ATPase in the ubiquitin system. Nat Cell Biol. 2012; 14:117–123. [PubMed: 22298039]
27. Vaz B, Halder S, Ramadan K. Role of p97/VCP (Cdc48) in genome stability. Front Genet. 2013; 4:60. [PubMed: 23641252]
28. Pelisch F, et al. Dynamic SUMO modification regulates mitotic chromosome assembly and cell cycle progression in Caenorhabditis elegans. Nature communications. 2014; 5:5485.
29. Merlet J, et al. The CRL2LRR-1 ubiquitin ligase regulates cell cycle progression during C. elegans development. Development. 2010; 137:3857–3866. [PubMed: 20978077]
30. Starostina NG, Simpliciano JM, McGuirk MA, Kipreos ET. CRL2(LRR-1) targets a CDK inhibitor for cell cycle control in C. elegans and actin-based motility regulation in human cells. Developmental cell. 2010; 19:753–764. [PubMed: 21074724]
31. Fullbright G, Rycenga HB, Gruber JD, Long DT. p97 Promotes a Conserved Mechanism of Helicase Unloading during DNA Cross-Link Repair. Mol Cell Biol. 2016; 36:2983–2994. [PubMed: 27644328]
32. Semlow DR, Zhang J, Budzowska M, Drohat AC, Walter JC. Replication-Dependent Unhooking of DNA Interstrand Cross-Links by the NEIL3 Glycosylase. Cell. 2016; 167:498–511 e414. [PubMed: 27693351]
33. Cuvier O, Stanojcic S, Lemaitre JM, Mechali M. A topoisomerase II-dependent mechanism for resetting replicons at the S-M-phase transition. Genes & development. 2008; 22:860–865. [PubMed: 18381889]
34. Bandau S, Knebel A, Gage ZO, Wood NT, Alexandru G. UBXN7 docks on neddylated cullin complexes using its UIM motif and causes HIF1alpha accumulation. BMC Biol. 2012; 10:36. [PubMed: 22537386]
35. Ossareh-Nazari B, Katsiarimpa A, Merlet J, Pintard L. RNAi-Based Suppressor Screens Reveal Genetic Interactions Between the CRL2LRR-1 E3-Ligase and the DNA Replication Machinery in Caenorhabditis elegans. G3 (Bethesda). 2016
36. Franz A, et al. CDC-48/p97 coordinates CDT-1 degradation with GINS chromatin dissociation to ensure faithful DNA replication. Mol Cell. 2011; 44:85–96. [PubMed: 21981920]

37. Franz A, et al. Chromatin-associated degradation is defined by UBXN-3/FAF1 to safeguard DNA replication fork progression. Nature communications. 2016; 7:10612.
38. Lee JJ, et al. Complex of Fas-associated factor 1 (FAF1) with valosin-containing protein (VCP)-Npl4-Ufd1 and polyubiquitinated proteins promotes endoplasmic reticulum-associated degradation (ERAD). J Biol Chem. 2013; 288:6998–7011. [PubMed: 23293021]
39. Menges CW, Altomare DA, Testa JR. FAS-associated factor 1 (FAF1): diverse functions and implications for oncogenesis. Cell Cycle. 2009; 8:2528–2534. [PubMed: 19597341]
40. Sharrock WJ, Sutherlin ME, Leske K, Cheng TK, Kim TY. Two distinct yolk lipoprotein complexes from Caenorhabditis elegans. J Biol Chem. 1990; 265:14422–14431. [PubMed: 2387862]
41. Gambus A, et al. A key role for Ctf4 in coupling the MCM2-7 helicase to DNA polymerase alpha within the eukaryotic replisome. EMBO J. 2009; 28:2992–3004. [PubMed: 19661920]
42. Sengupta S, van Deursen F, de Piccoli G, Labib K. Dpb2 integrates the leading-strand DNA polymerase into the eukaryotic replisome. Current biology: CB. 2013; 23:543–552. [PubMed: 23499531]
43. Brenner S. The genetics of Caenorhabditis elegans. Genetics. 1974; 77:71–94. [PubMed: 4366476]
44. Edgley ML, Baillie DL, Riddle DL, Rose AM. Genetic balancers. WormBook. 2006:1–32.
45. Timmons L, Fire A. Specific interference by ingested dsRNA. Nature. 1998; 395:854. [PubMed: 9804418]
46. Gillespie PJ, Gambus A, Blow JJ. Preparation and use of Xenopus egg extracts to study DNA replication and chromatin associated proteins. Methods. 2012; 57:203–213. [PubMed: 22521908]
47. Gambus A, Khoudoli GA, Jones RC, Blow JJ. MCM2-7 form double hexamers at licensed origins in Xenopus egg extract. J Biol Chem. 2011; 286:11855–11864. [PubMed: 21282109]
48. Khoudoli GA, et al. Temporal profiling of the chromatin proteome reveals system-wide responses to replication inhibition. Curr Biol. 2008; 18:838–843. [PubMed: 18514518]
49. Prokhorova TA, Blow JJ. Sequential MCM/P1 subcomplex assembly is required to form a heterohexamer with replication licensing activity. J Biol Chem. 2000; 275:2491–2498. [PubMed: 10644704]
50. Heubes S, Stemmann O. The AAA-ATPase p97-Ufd1-Npl4 is required for ERAD but not for spindle disassembly in Xenopus egg extracts. J Cell Sci. 2007; 120:1325–1329. [PubMed: 17374636]
51. Walter JC. Evidence for sequential action of cdc7 and cdk2 protein kinases during initiation of DNA replication in Xenopus egg extracts. J Biol Chem. 2000; 275:39773–39778. [PubMed: 11005825]
52. Hodgson B, Li A, Tada S, Blow JJ. Geminin becomes activated as an inhibitor of Cdt1/RLF-B following nuclear import. Curr Biol. 2002; 12:678–683. [PubMed: 11967157]
53. Lee DW, et al. The Dac-tag, an affinity tag based on penicillin-binding protein 5. Anal Biochem. 2012; 428:64–72. [PubMed: 22705378]

Europe PMC Funders Author Manuscripts

Europe PMC Funders Author Manuscripts

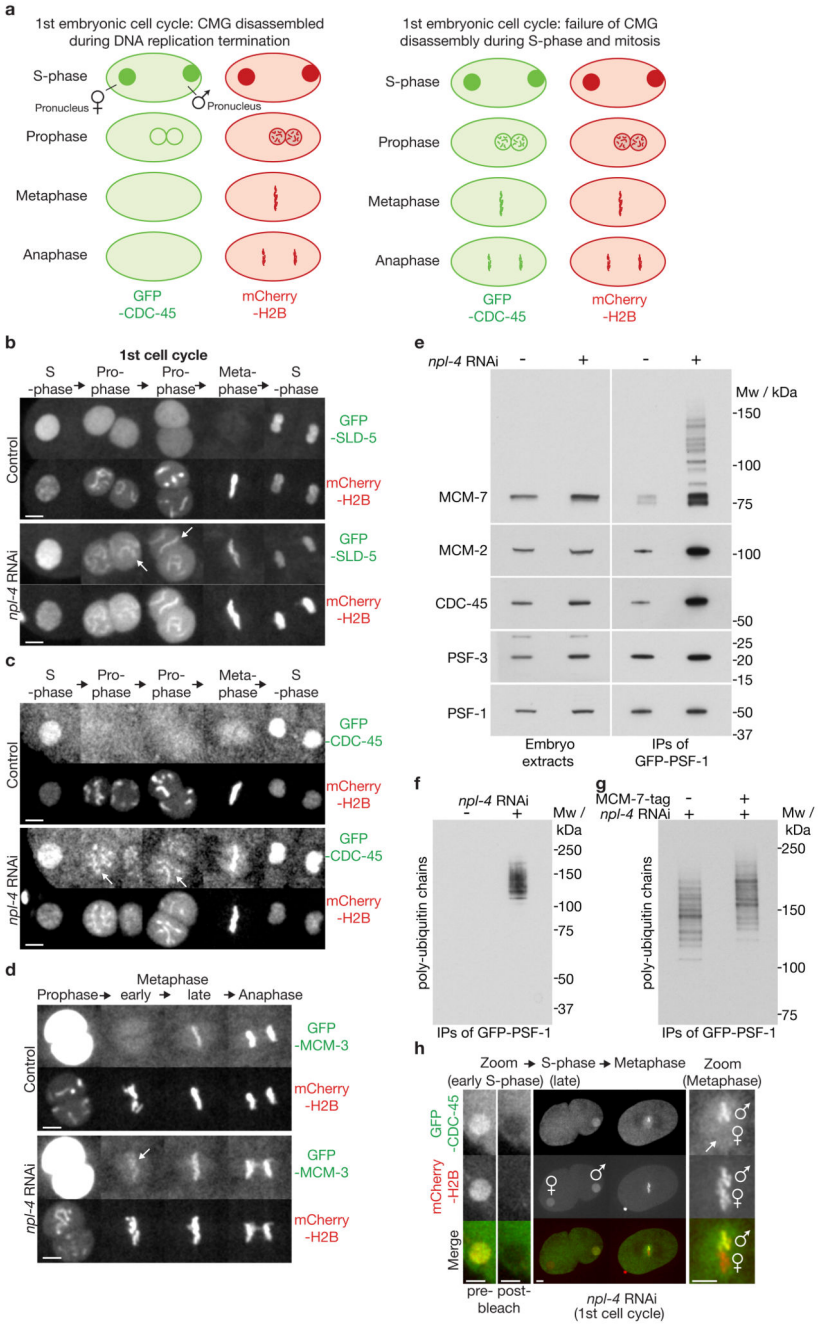

Figure 1. The CDC-48 co-factor NPL-4 is required for CMG helicase disassembly during S-phase in the *C. elegans* early embryo.

(**a**) Illustration of a live-embryo assay for CMG helicase disassembly, comparing control embryos (‘normal CMG disassembly’) with mutant embryos (‘defective CMG disassembly’). Note that the two nuclei derived from oogenesis and spermatogenesis – referred to in this manuscript as the female and male pronuclei - move together during prophase of the first cell cycle. Following nuclear envelope breakdown, the ‘male’ and ‘female’ sets of chromosomes then intermingle during metaphase. (**b**) Timelapse video microscopy of the first cell cycle in embryos expressing GFP-SLD-5 and mCherry-

HistoneH2B, either untreated or exposed to *npl-4* RNAi. The female pronucleus is shown during S-phase, before convergence with the male pronucleus. Prophase begins during migration of the pronuclei. The arrows indicate examples of persistence of GFP-SLD-5 on chromatin during prophase after depletion of NPL-4. (**c**) Equivalent analysis for embryos expressing GFP-CDC-45. (**d**) Equivalent data for embryos expressing GFP-MCM-3. The arrow indicates the small pool of GFP-MCM-3 that remains on chromatin during early metaphase after depletion of NPL-4. (**e**) Homozygous *GFP-psf-1 / GFP-psf-1* worms were exposed to *npl-4* RNAi or left untreated. Embryos were then isolated and used to generate whole-embryo extracts, before immunoprecipitation of GFP-PSF-1. The indicated proteins were monitored by immunoblotting. (**f**) The same samples were separated in a 4-12% gradient gel, before immunoblotting with an antibody to poly-ubiquitin chains. (**g**) Equivalent *npl-4* RNAi experiment comparing control worms with homozygous *mcm7-5FLAG-9His* embryos generated by CRISPR-Cas9. The samples were separated in a 3-8% gradient gel, before immunoblotting with antibody to poly-ubiquitin chains. (**h**) Timelapse video microscopy of an *npl-4* RNAi embryo expressing GFP-CDC-45 and mCherry-HistoneH2B. The GFP signal in the female pronucleus was photo-bleached during early S-phase and then monitored in the subsequent mitosis. Lack of recovery of the GFP signal on ‘female’ chromosomes, compared to the unbleached control male pronucleus, indicated that GFP-CDC45 persists on chromatin after S-phase rather than being reloaded, in embryos lacking NPL-4. The scale bars correspond to 5μm. Unprocessed scans of key immunoblots are shown in Supplementary Figure 8.

Europe PMC Funders Author Manuscripts

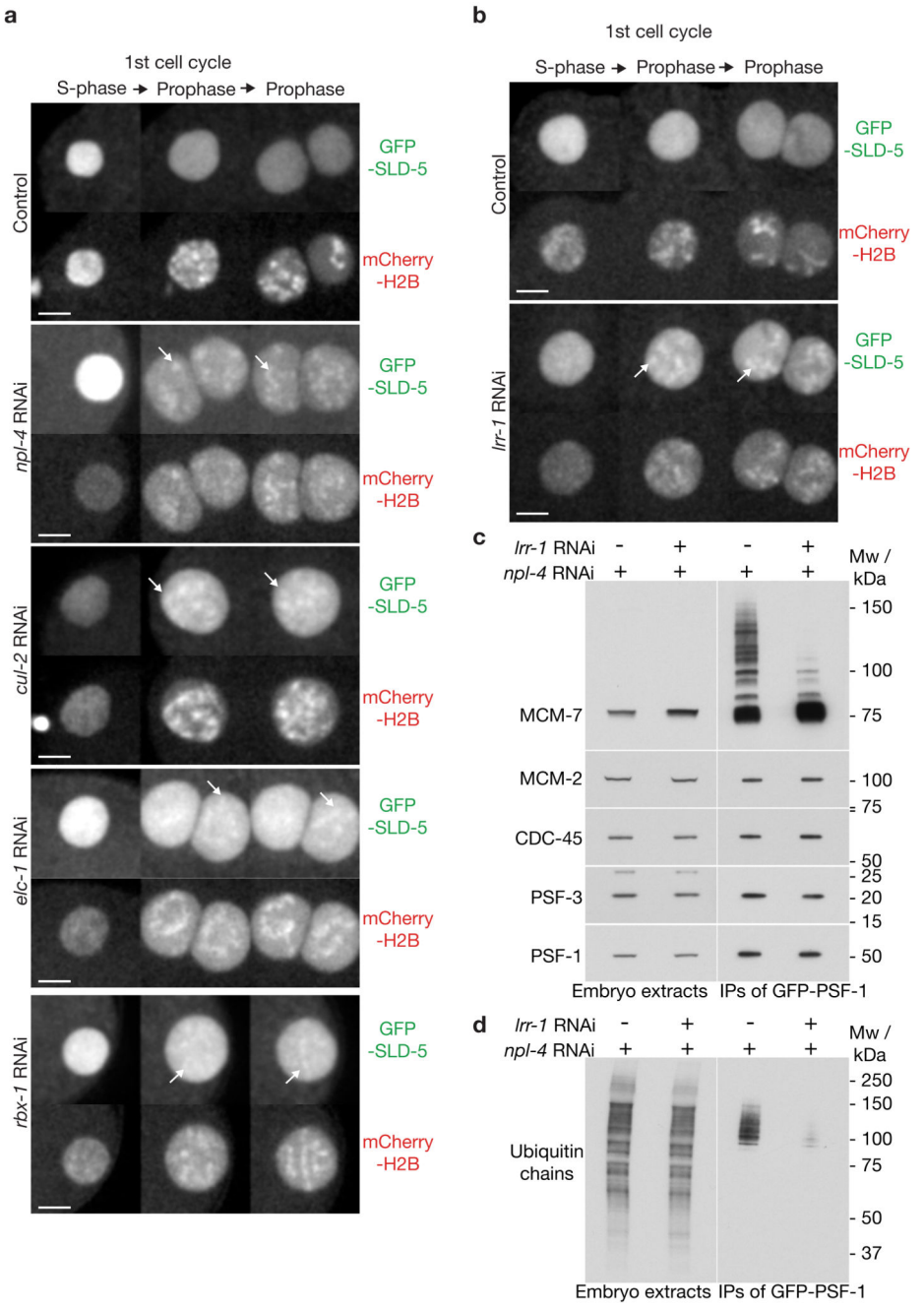

Figure 2. CUL-2^{LRR-1} is required for CMG helicase disassembly during S-phase in *C. elegans*.

(**a-b**) Embryos from *GFP-sld-5 mCherry-H2B* worms were exposed to the indicated RNAi and processed as in Figure 1b. Timelapse images are shown from S-phase to mid-prophase. Five embryos were examined for each treatment and all behaved equivalently. Arrows denote examples of persistence of GFP-SLD-5 on prophase chromatin and scale bars correspond to 5μm. (**c-d**) Embryos from homozygous *GFP-psf-1 / GFP-psf-1* worms were exposed to the indicated RNAi and processed as in Figure 1e-f. Unprocessed scans of key immunoblots are shown in Supplementary Figure 8.

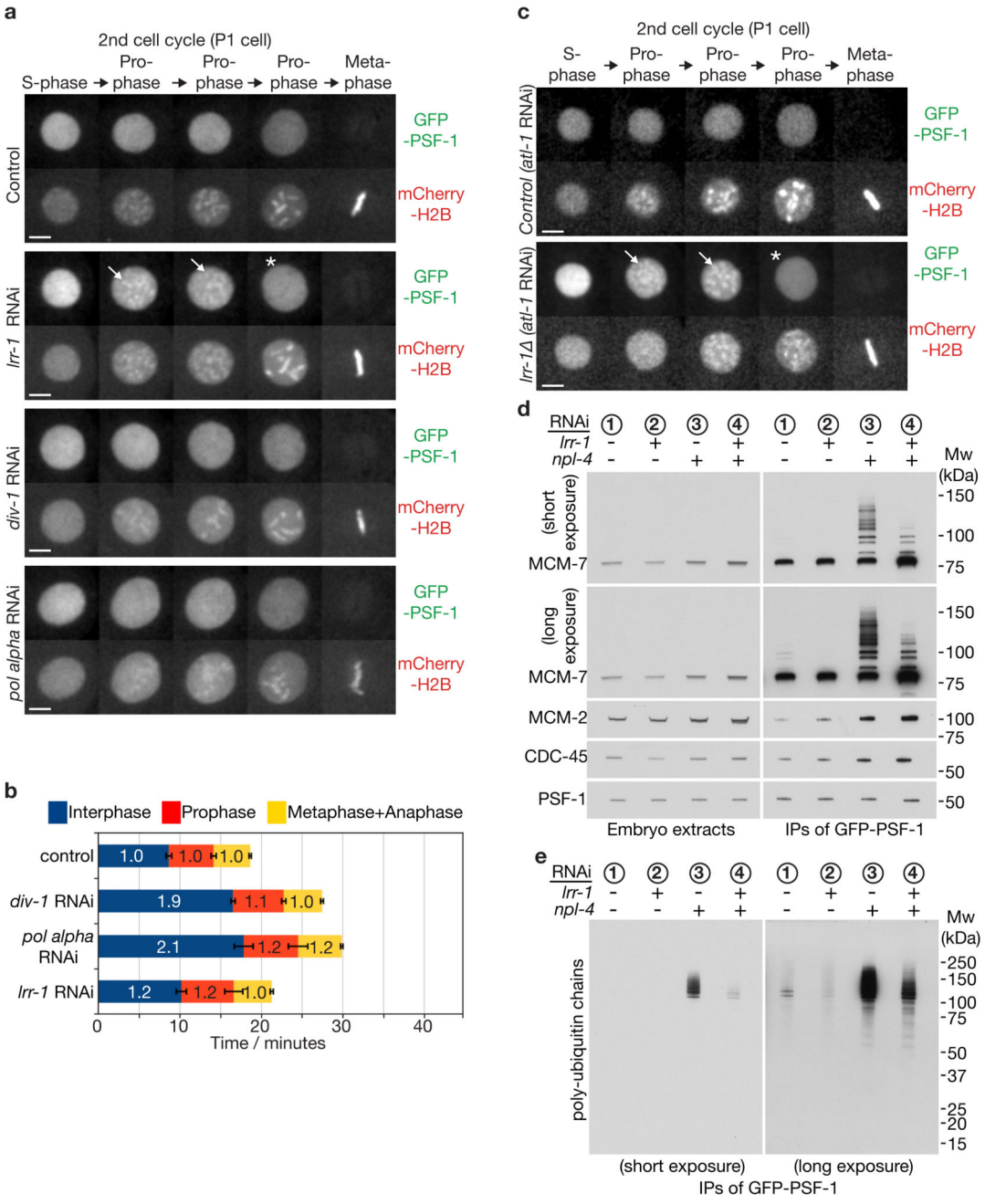

Figure 3. A mitotic pathway for CMG helicase disassembly is revealed in the absence of CUL-2^{LRR-1}.

(**a**) Embryos from *GFP-psf-1 mCherry-H2B* worms were exposed to the indicated RNAi treatments, or empty vector in the control, and then processed as in Figure 1b, except that the figure depicts data from the second embryonic cell cycle (P1 cell). Timelapse images are shown from S-phase to metaphase. GFP-PSF1 initially persists on prophase chromatin following depletion of LRR-1 (the arrows denote examples), before being released in late prophase (indicated by asterisk). Scale bars correspond to 5μm. (**b**) The duration of the

indicated cell cycle phases for the experiment in (a) were measured as described in Methods. The data are expressed relative to the length of the corresponding period in control embryos, and represent the mean values (n = 5 embryos; the lines on the boundary of each cell cycle phase indicate standard deviations from the mean). (**c**) Worms homozygous for *GFP-psf-1* and *lrr-1Δ* were grown in parallel to the equivalent heterozygote (control), as described in Methods. After exposure to *atl-1* RNAi (this allows homozygous *lrr-1Δ* germ cells to proceed with meiosis), the resultant embryos were processed as above. The images depict the second embryonic cell cycle (P1 cell), showing persistent association of GFP-PSF-1 with chromatin during prophase (arrows), before release in late prophase (asterisk). (**d-e**) Homozygous *GFP-psf-1* worms were exposed to the indicated RNAi. Embryos were then isolated and processed as in Figure 1e-f. Unprocessed scans of key immunoblots are shown in Supplementary Figure 8.

Europe PMC Funders Author Manuscripts

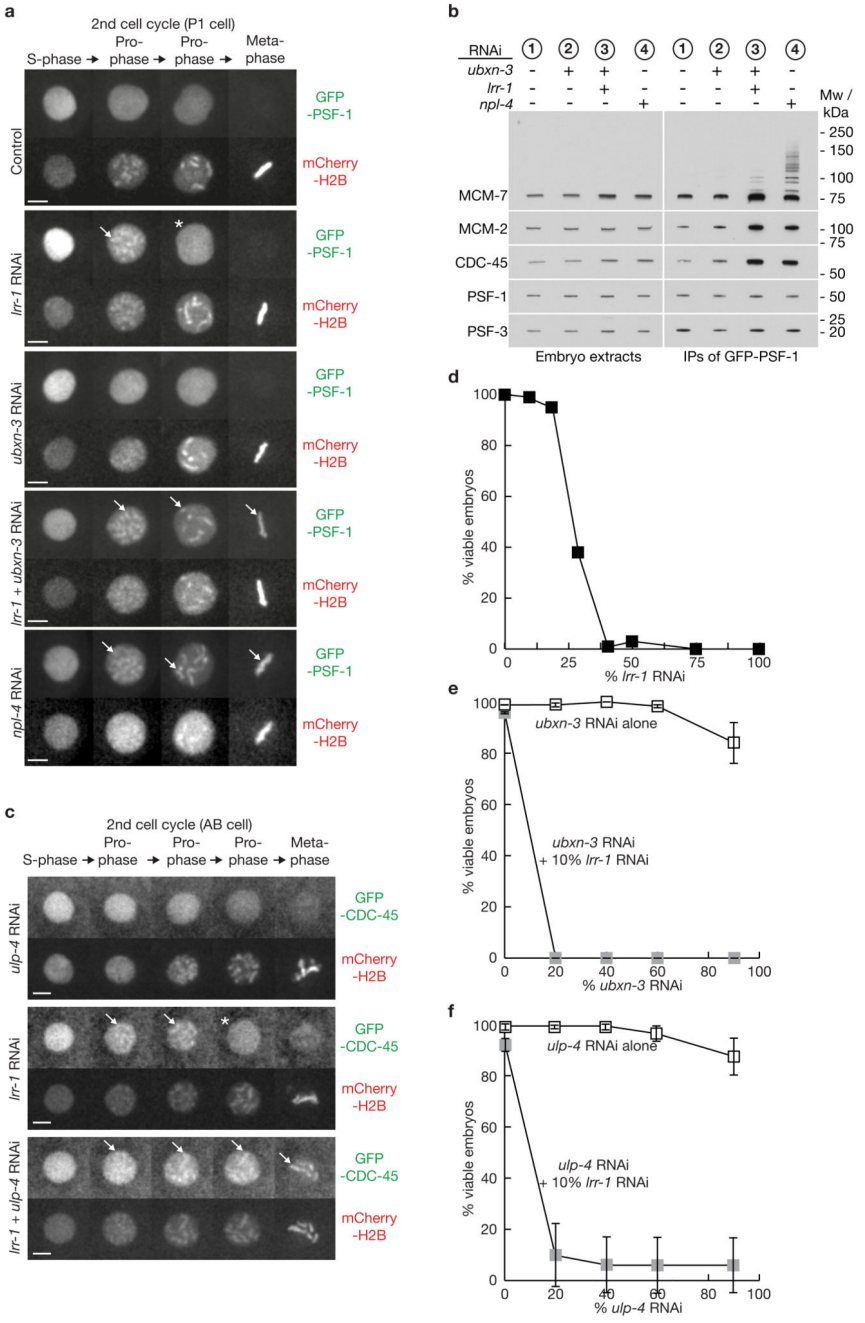

Figure 4. The mitotic CMG helicase disassembly pathway requires UBXN-3 and is modulated by the SUMO protease ULP-4, both of which become essential when LRR-1 is depleted.

(**a**) Embryos from *GFP-psf-1 mCherry-H2B* worms were exposed to the indicated RNAi and processed as in Figure 3a. The arrows indicate persistent association of GFP-PSF1 with mitotic chromatin (throughout mitosis in the case of RNAi to *npl-4*, or after simultaneous RNAi to *lrr-1 + ubxn-3*), whereas the asterisk denotes release of GFP-PSF-1 from chromatin in late prophase in embryos treated only with *lrr-1* RNAi. The scale bars correspond to 5μm. (**b**) Homozygous *GFP-psf-1* worms were exposed to the indicated RNAi and isolated

Europe PMC Funders Author Manuscripts

embryos were then processed as in Figure 1e. (**c**) Embryos from *GFP-cdc-45 mCherry-H2B* worms were exposed to the indicated RNAi and processed as above. The data correspond to the AB cell in the second cell cycle, in which *lrr-1 ulp-4* double RNAi leads to persistence of GFP-CDC-45 until at or after nuclear envelope breakdown (8 of 9 embryos tested). (**d**) Worms were fed on plates where the indicated proportion of bacteria expressed *lrr-1* double-stranded RNAi, and embryonic viability was measured as described in Methods (for each timepoint, 69-94 embryos were examined from five adult worms). (**e**) Worms were fed on the indicated proportion of bacteria expressing *ubxn-3* RNAi, either alone or in combination with 10% bacteria expressing *lrr-1* RNAi. The data represent the mean values (n = 3 independent experiments; for each timepoint, 70-100 embryos were examined from five adult worms), with the indicated standard deviations from the mean value. (**f**) Similar experiment involving increasing doses of *ulp-4* RNAi, with or without 10% *lrr-1* RNAi (n = 3 independent experiments; for each timepoint, 70-100 embryos were examined from five adult worms). Unprocessed scans of key immunoblots are shown in Supplementary Figure 8.

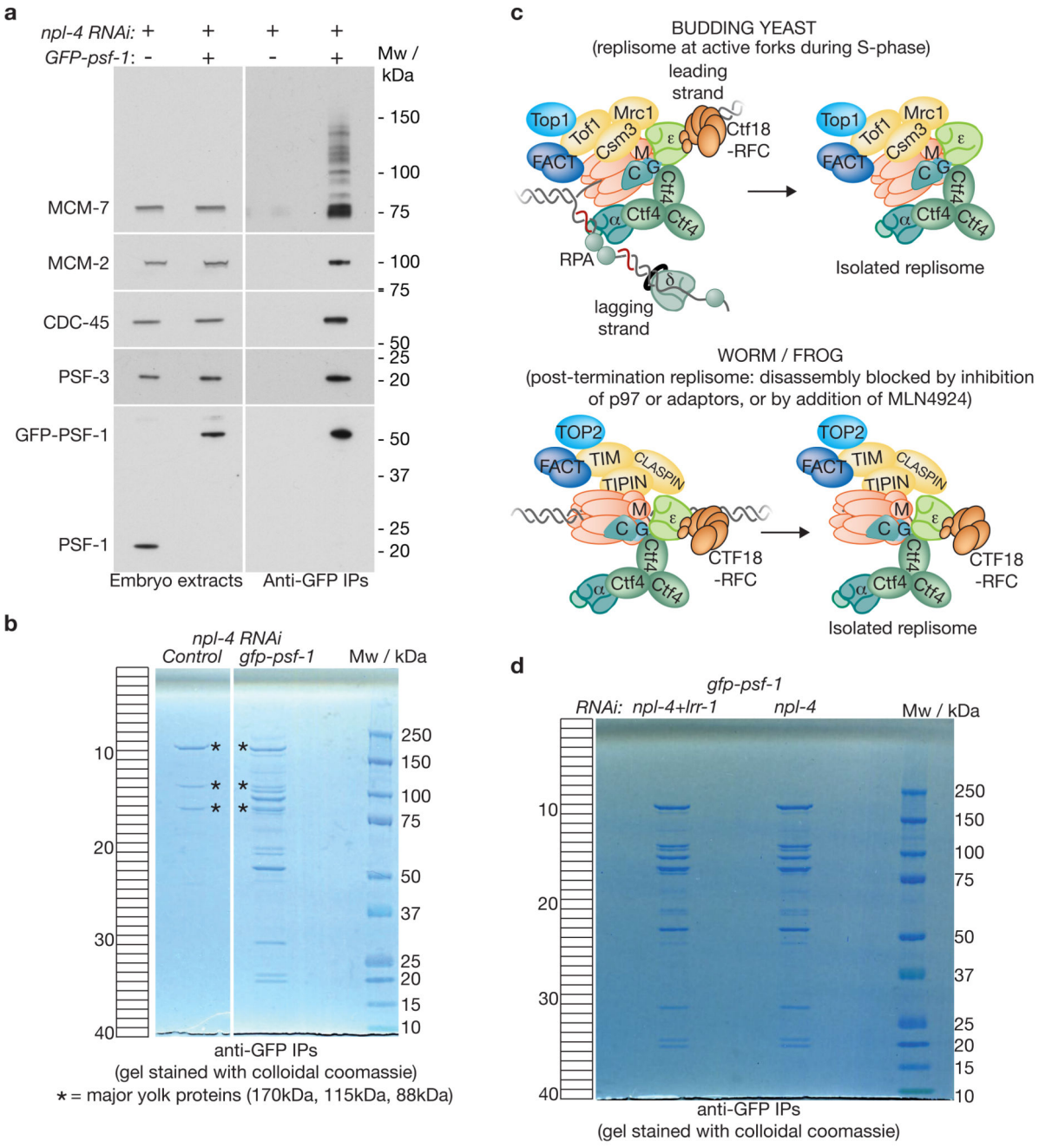

Figure 5. Isolation of the post-termination worm replisome.

(**a**) Control or homozygous *GFP-psf-1* worms were exposed to *npl-4* RNAi before being processed as described above for Figure 4. The purified samples were monitored by SDS-PAGE and immunoblotting of the indicated components of the CMG helicase. (**b**) The remainder of the samples were then resolved in a 4-12% gradient gel, which was stained with colloidal coomassie. The major contaminants in both samples (marked with asterisks) represent the four major yolk proteins of the worm early embryo40. Each lane was cut into 40 bands as indicated, before analysis of protein content by mass spectrometry (see

Supplementary Table 2). (**c**) Comparison of the replisome isolated from active replication forks in budding yeast 1, 41, 42, with the isolated post-termination replisome from worm and frog (this study). For simplicity, some of the proteins that act at forks, but that are not present in the isolated replisome, have been omitted. In addition, Mcm10 has been excluded, since its status at forks and its association with the isolated replisome remain unclear (absent from isolated yeast and worm replisomes under physiological conditions, but co-purifying with frog MCM-3 from digested chromatin post-termination). (**d**) Comparison of isolated replisome material for the experiment in Supplementary Table 3 (worms treated with *npl-4* RNAi or *npl-4 lrr-1* double RNAi). Unprocessed scans of key immunoblots are shown in Supplementary Figure 8.

Europe PMC Funders Author Manuscripts

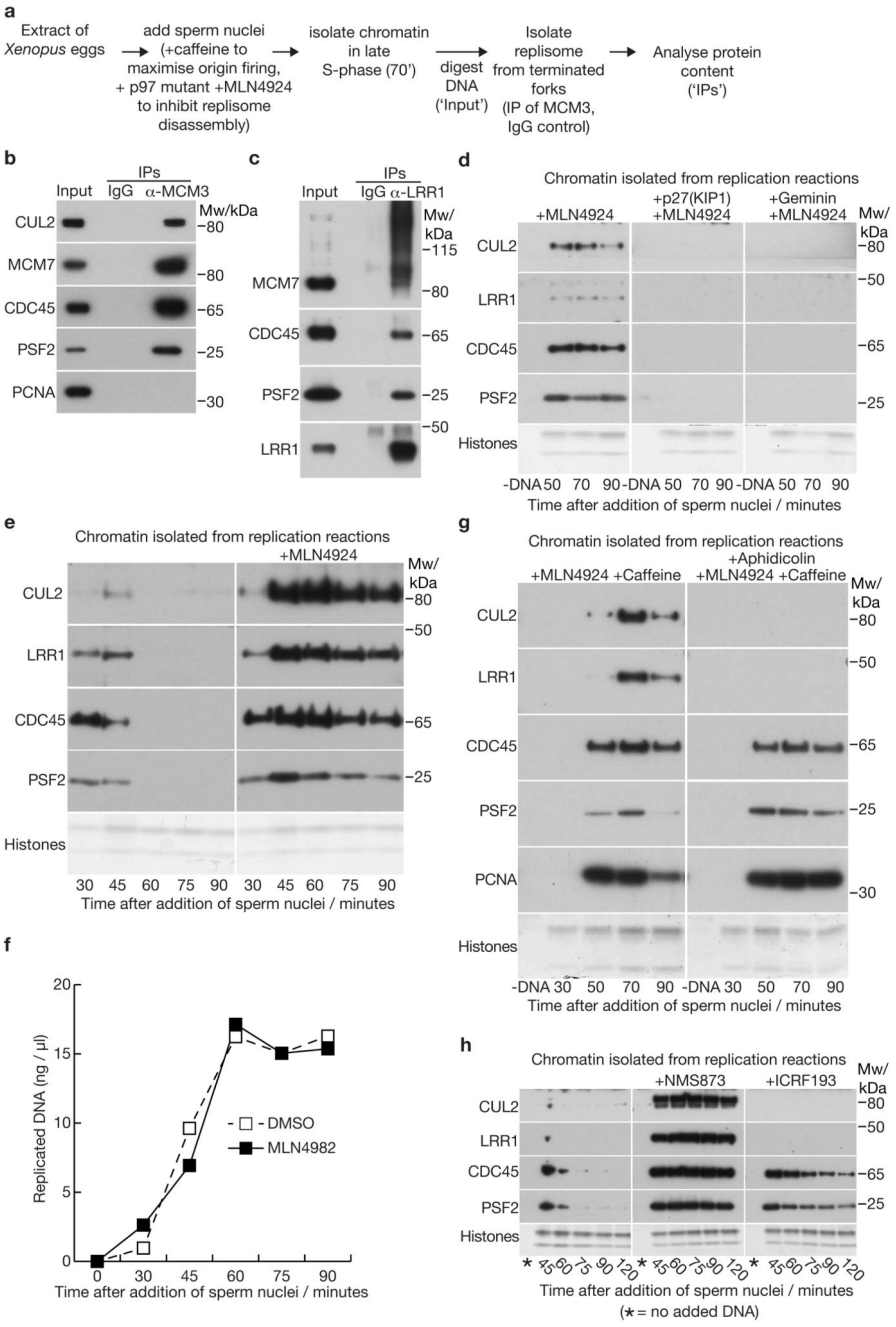

Figure 6. CUL2^{LRR1} associates with the post-termination vertebrate replisome and is recruited to chromatin during DNA replication termination in *Xenopus* egg extracts.

(**a**) Experimental scheme for isolation of proteins associated with the CMG helicase after termination in the absence of replisome disassembly, in extracts of *Xenopus laevis* eggs. (**b**) Immunoblots of input and the indicated IP samples for the experiment in (a). (**c**) Replisome disassembly was inhibited with the p97 inhibitor NMS873, and LRR1 was then isolated from digested chromatin at the 70' timepoint, in parallel with a control IP with IgG, before detection of the indicated proteins by immunoblotting. (**d**) Chromatin association of the

indicated factors was monitored by immunoblotting, at the indicated timepoints after addition of sperm chromatin to egg extracts (except for the -DNA sample that lacked chromatin). Where indicated, replication initiation was blocked by addition of p27(KIP1) or Geminin. The neddylase inhibitor MLN4924 was added to all samples to block replisome disassembly. (**e**) Timecourse experiment comparing chromatin-bound factors in the absence or presence of the neddylation inhibitor MLN4924. (**f**) Replication kinetics were monitored for the experiment in (e), by incorporation of radiolabelled α-dATP into newly synthesised DNA (see also Supplementary Figure 5b; source data for repeats of this experiment are included in Supplementary Table 6). (**g**) Inhibition of DNA synthesis blocks association of $CUL2^{LRR1}$ with chromatin. DNA synthesis was inhibited with the DNA polymerase inhibitor aphidicolin. Caffeine was added to inactivate the S-phase checkpoint, which otherwise would have reduced the level of CMG on chromatin +Aphidicolin. (**h**) Analogous experiment to that in (e), showing that CUL2-LRR1 accumulated on chromatin with CMG when replisome disassembly was blocked by the p97 inhibitor NMS873, but chromatin recruitment of CUL2-LRR1 was inhibited if DNA replication termination was delayed by addition of the TOPO2 inhibitor ICRF193. Unprocessed scans of key immunoblots are shown in Supplementary Figure 8.

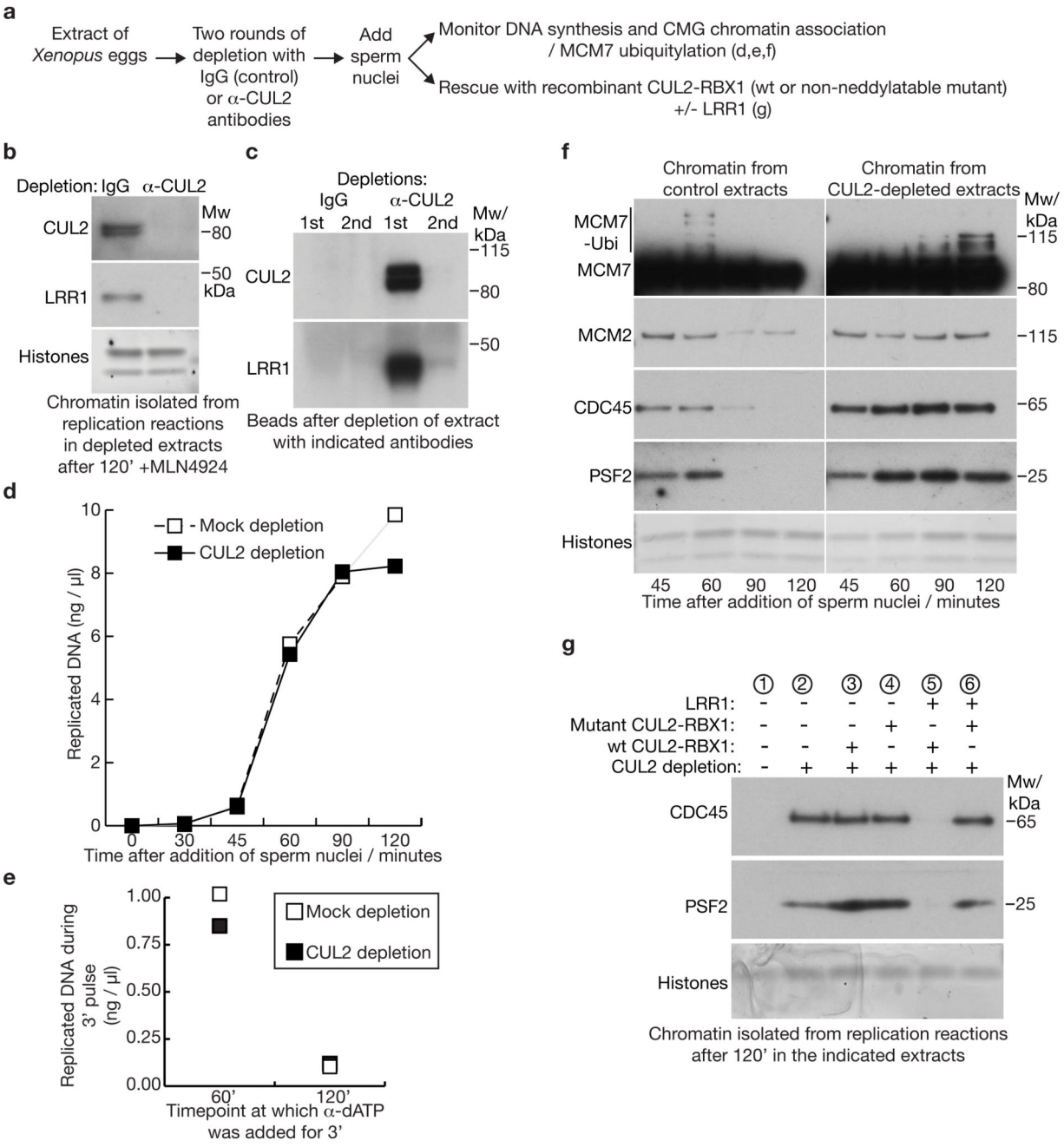

Figure 7. Active CUL2^{LRR1} is required for extraction of CMG components from chromatin during DNA replication termination in *Xenopus* egg extracts.

(**a**) Experimental scheme. (**b**) Replication reactions were performed in the presence of MLN4924 to stabilise CUL2^{LRR1} on chromatin during DNA replication termination in mock-depleted extracts (treated with two rounds of IgG-beads). In contrast, neither CUL2 nor LRR1 were detected on chromatin in CUL2-depleted extracts, confirming the efficiency of the depletion. (**c**) Depletion of CUL2 also removes LRR1 from the extract (the panel shows immunoblots of the antibody-coupled beads after each of the two rounds of

Europe PMC Funders Author Manuscripts

depletion). (**d**) Kinetics of DNA synthesis in extracts subjected to two rounds of immunoprecipitation with control IgG ('mock depletion') or with antibodies to Hs_CUL2-RBX1 ('CUL2 depletion', see Methods). Source data for repeats of this experiment are included in Supplementary Table 6. (**e**) In an analogous experiment, replication reactions were performed in 'mock-depleted' and CUL-depleted extracts. A pulse of α-dATP was added for 3' at either the 60' or 120' timepoints, and the incorporation of radiolabel into nascent DNA was monitored after isolation of total DNA, indicating that replication proceeded and completed with similar kinetics in both extracts, consistent with the data in (d). (**f**) Kinetics of chromatin association of the indicated factors for the same experiment shown in (a-b). Note that the MCM7 immunoblot is over-exposed in order to reveal the ubiquitylated forms of the protein. (**g**) Mock-depleted or CUL2-depleted extracts were supplemented with the indicated recombinant proteins (X.l. LRR1, wt/mutant Hs_CUL2-RBX1 – see Methods), and chromatin was isolated from the 120' timepoint in a similar experiment to that described above. Unprocessed scans of key immunoblots are shown in Supplementary Figure 8.